

QPSK Waveform for MIMO Radar with Spectrum Sharing Constraints

Awais Khawar, Ahmed Abdelhadi, and T. Charles Clancy

Abstract

Multiple-input multiple-output (MIMO) radar is a relatively new concept in the field of radar signal processing. Many novel MIMO radar waveforms have been developed by considering various performance metrics and constraints. In this paper, we show that finite alphabet constant-envelope (FACE) quadrature-pulse shift keying (QPSK) waveforms can be designed to realize a given covariance matrix by transforming a constrained nonlinear optimization problem into an unconstrained nonlinear optimization problem. In addition, we design QPSK waveforms in a way that they don't cause interference to a cellular system, by steering nulls towards a selected base station (BS). The BS is selected according to our algorithm which guarantees minimum degradation in radar performance due to null space projection (NSP) of radar waveforms. We design QPSK waveforms with spectrum sharing constraints for a stationary and moving radar platform. We show that the waveform designed for stationary MIMO radar matches the desired beampattern closely, when the number of BS antennas N^{BS} is considerably less than the number of radar antennas M , due to quasi-static interference channel. However, for moving radar the difference between designed and desired waveforms is larger than stationary radar, due to rapidly changing channel.

Index Terms

MIMO Radar, Constant Envelope Waveform, QPSK, Spectrum Sharing

I. INTRODUCTION

An interesting concept for next generation of radars is multiple-input multiple-output (MIMO) radar systems; this has been an active area of research for the last couple of years [1]. MIMO radars have been classified into widely-spaced [2], where antenna elements are placed widely apart, and colocated [3], where antenna elements are placed next to each other. MIMO radars can transmit multiple signals, via its antenna elements, that can be different from

Awais Khawar (awais@vt.edu) is with Virginia Polytechnic Institute and State University, Arlington, VA, 22203.

Ahmed Abdelhadi (aabdelhadi@vt.edu) is with Virginia Polytechnic Institute and State University, Arlington, VA, 22203.

T. Charles Clancy (tcc@vt.edu) is with Virginia Polytechnic Institute and State University, Arlington, VA, 22203.

This work was supported by DARPA under the SSPARC program. Contract Award Number: HR0011-14-C-0027. The views expressed are those of the author and do not reflect the official policy or position of the Department of Defense or the U.S. Government.

Distribution Statement A: Approved for public release; distribution is unlimited.

each other, thus, resulting in waveform diversity. This gives MIMO radars an advantage over traditional phased-array radar systems which can only transmit scaled versions of single waveform and, thus, can't exploit waveform diversity.

Waveforms with constant-envelope (CE) are very desirable, in radar and communication system, from an implementation perspective, i.e., they allow power amplifiers to operate at or near saturation levels. CE waveforms are also popular due to their ability to be used with power efficient class C and class E power amplifiers and also with linear power amplifiers with no average power back-off into power amplifier. As a result, various researchers have proposed CE waveforms for communication systems; for example, CE multi-carrier modulation waveforms [4], such as CE orthogonal frequency division multiplexing (CE-OFDM) waveforms [5]; and radar systems, for example, CE waveforms [6], CE binary-phase shift keying (CE-BPSK) waveforms [7], and CE quadrature-phase shift keying (CE-QPSK) waveforms [8].

Existing radar systems, depending upon their type and use, can be deployed any where between 3 MHz to 100 GHz of radio frequency (RF) spectrum. In this range, many of the bands are very desirable for international mobile telecommunication (IMT) purposes. For example, portions of the 700-3600 MHz band are in use by various second generation (2G), third generation (3G), and fourth generation (4G) cellular standards throughout the world. It is expected that mobile traffic volume will continue to increase as more and more devices will be connected to wireless networks. The current allocation of spectrum to wireless services is inadequate to support the growth in traffic volume. A solution to this spectrum congestion problem was presented in a report by President's Council of Advisers on Science and Technology (PCAST), which advocated to *share* 1000 MHz of government-held spectrum [9]. As a result, in the United States (U.S.), regulatory efforts are underway, by the Federal Communications Commission (FCC) along with the National Telecommunications and Information Administration (NTIA), to share government-held spectrum with commercial entities in the frequency band 3550-3650 MHz [10]. In the U.S., this frequency band is currently occupied by various services including radio navigation services by radars. The future of spectrum sharing in this band depends on novel interference mitigation methods to protect radars and commercial cellular systems from each others' interference [?], [?], [11]. Radar waveform design with interference mitigation properties is one way to address this problem, and this is the subject of this paper.

A. Related Work

Transmit beampattern design problem, to realize a given covariance matrix subject to various constraints, for MIMO radars is an active area of research; many researchers have proposed algorithms to solve this beampattern matching problem. Fuhrmann et al. proposed waveforms with arbitrary cross-correlation matrix by solving beampattern optimization problem, under the constant-modulus constraint, using various approaches [12]. Aittomaki et al. proposed to solve beampattern optimization problem under the total power constraint as a least squares problem [13]. Gong et al. proposed an optimal algorithm for omnidirectional beampattern design problem with the constraint to have sidelobes smaller than some predetermined threshold values [14]. Hua et al. proposed transmit beampatterns with constraints on ripples, within the energy focusing section, and the transition bandwidth [15].

However, many of the above approaches don't consider designing waveforms with finite alphabet and constant-envelope property, which is very desirable from an implementation perspective. Ahmed et al. proposed a method to synthesize covariance matrix of BPSK waveforms with finite alphabet and constant-envelope property [7]. They also proposed a similar solution for QPSK waveforms but it didn't satisfy the constant-envelope property. A method to synthesize covariance matrix of QPSK waveforms with finite alphabet and constant-envelope property was proposed by Sodagari et al. [8]. However, they did not prove that such a method is possible. We prove the result in this paper and show that it is possible to synthesize covariance matrix of QPSK waveforms with finite alphabet and constant-envelope property.

As introduced earlier due to the congestion of frequency bands future communication systems will be deployed in radar bands. Thus, radars and communication systems are expected to share spectrum without causing interference to each other. For this purpose, radar waveforms should be designed in such a way that they not only mitigate interference to them but also mitigate interference by them to other systems [16], [17]. Transmit beampattern design by considering the spectrum sharing constraints is a fairly new problem. Sodagari et al. have proposed BPSK and QPSK transmit beampatterns by considering the constraint that the designed waveforms do not cause interference to a single communication system [8]. This approach was extended to multiple communication systems, cellular system with multiple base stations, by Khawar et al. for BPSK transmit beampatterns [18], [19]. We extend this approach and consider optimizing QPSK transmit beampatterns for a cellular system with multiple base stations.

B. Our Contributions

In this paper, we make contributions in the areas of:

- **Finite alphabet constant-envelope QPSK waveform:** In this area of MIMO radar waveform design, we make the following contribution: we prove that covariance matrix of finite alphabet constant-envelope QPSK waveform is positive semi-definite and the problem of designing waveform via solving a constrained optimization problem can be transformed into an un-constrained optimization problem.
- **MIMO radar waveform with spectrum sharing constraints:** We design MIMO radar waveform for spectrum sharing with cellular systems. We modify the newly designed QPSK radar waveform in a way that it doesn't cause interference to communication system. We design QPSK waveform by considering the spectrum sharing constraints, i.e., the radar waveform should be designed in such a way that a cellular system experiences zero interference. We consider two cases: first, stationary maritime MIMO radar is considered which experiences a stationary or slowly moving interference channel. For this type of radar, waveform is designed by including the constraints in the unconstrained nonlinear optimization problem, due to the tractability of the constraints. Second, we consider a moving maritime MIMO radar which experiences interference channels that are fast enough not to be included in the optimization problem due to their intractability. For this type of radar, FACE QPSK waveform is designed which is then projected onto the null space of interference channel before transmission.

TABLE I
TABLE OF NOTATIONS

Notation	Description
$\tilde{\mathbf{x}}(n)$	Transmitted QPSK radar waveform
$\mathbf{a}(\theta_k)$	Steering vector to steer signal to target angle θ_k
$\tilde{\mathbf{r}}_k(n)$	Received radar waveform from target at θ_k
$\tilde{\mathbf{R}}$	Correlation matrix of QPSK waveforms
$\mathbf{s}_j(n)$	Signal transmitted by the j^{th} UE in the i^{th} cell
\mathcal{L}_i	Total number of user equipments (UEs) in the i^{th} cell
\mathcal{K}	Total number of BSs
M	Radar transmit/receive antennas
N_{BS}	BS transmit/receive antennas
N_{UE}	UE transmit/receive antennas
\mathbf{H}_i	i^{th} interference channel
H_n	Hermite Polynomial
$\mathbf{y}_i(n)$	Received signal at the i^{th} BS
\mathbf{P}_i	Projection matrix for the i^{th} channel

C. Organization

This paper is organized as follows. System model, which includes radar, communication system, interference channel, and cooperative RF environment model is discussed in Section II. Section III introduces finite alphabet constant-envelope beampattern matching design problem. Section IV introduces QPSK radar waveforms and Section V provides a proof of FACE QPSK waveform. Section VI discusses spectrum sharing architecture along with BS selection and projection algorithm. Section VII designs QPSK waveforms with spectrum sharing constraints for stationary and moving radar platforms. Section VIII discusses simulation setup and results. Section IX concludes the paper.

D. Notations

Bold upper case letters, \mathbf{A} , denote matrices while bold lower case letters, \mathbf{a} , denote vectors. The m^{th} column of matrix is denoted by \mathbf{a}_m . For a matrix \mathbf{A} , the conjugate and conjugate transposition are respectively denoted by \mathbf{A}^* and \mathbf{A}^H . The m^{th} row and n^{th} column element is denoted by $\mathbf{A}(m, n)$. Real and complex, vectors and matrices are denoted by operators $\Re(\cdot)$ and $\Im(\cdot)$, respectively. A summary of notations is provided in Table I.

II. SYSTEM MODEL

In this section, we introduce our system models for MIMO radar and cellular system. In addition, we introduce the cooperative RF sharing environment between radar and cellular system along with the definition of interference channel.

A. Radar Model

We consider waveform design for a colocated MIMO radar mounted on a ship. The radar has M colocated transmit and receive antennas. The inter-element spacing between antenna elements is on the order of half the wavelength. The radars with colocated elements give better spatial resolution and target parameter estimation as compared to radars with widely spaced antenna elements [2], [3].

B. Communication System

We consider a MIMO cellular system, with \mathcal{K} base stations, each equipped with N_{BS} transmit and receive antennas, with the i^{th} BS supporting \mathcal{L}_i user equipments (UEs). Moreover, the UEs are also multi-antenna systems with N_{UE} transmit and receive antennas. If $\mathbf{s}_j(n)$ is the signals transmitted by the j^{th} UE in the i^{th} cell, then the received signal at the i^{th} BS receiver can be written as

$$\mathbf{y}_i(n) = \sum_j \mathbf{H}_{i,j} \mathbf{s}_j(n) + \mathbf{w}(n), \quad \text{for } 1 \leq i \leq \mathcal{K} \text{ and } 1 \leq j \leq \mathcal{L}_i$$

where $\mathbf{H}_{i,j}$ is the channel matrix between the i^{th} BS and the j^{th} user and $\mathbf{w}(n)$ is the additive white Gaussian noise.

C. Interference Channel

In our spectrum sharing model, radar shares \mathcal{K} interference channels with cellular system. Let's define the i^{th} interference channel as

$$\mathbf{H}_i \triangleq \begin{bmatrix} h_i^{(1,1)} & \dots & h_i^{(1,M)} \\ \vdots & \ddots & \vdots \\ h_i^{(N_{\text{BS}},1)} & \dots & h_i^{(N_{\text{BS}},M)} \end{bmatrix} \quad (N_{\text{BS}} \times M) \quad (1)$$

where $i = 1, 2, \dots, \mathcal{K}$, and $h_i^{(l,k)}$ denotes the channel coefficient from the k^{th} antenna element at the MIMO radar to the l^{th} antenna element at the i^{th} BS. We assume that elements of \mathbf{H}_i are independent, identically distributed (i.i.d.) and circularly symmetric complex Gaussian random variables with zero-mean and unit-variance, thus, having a i.i.d. Rayleigh distribution.

D. Cooperative RF Environment

Spectrum sharing between radars and communication systems can be envisioned in two types of RF environments, i.e., military radars sharing spectrum with military communication systems, we characterize it as *Mil2Mil* sharing and military radars sharing spectrum with commercial communication systems, we characterize it as *Mil2Com* sharing. In *Mil2Mil* or *Mil2Com* sharing, interference-channel state information (ICSI) can be provided to radars via feedback by military/commercial communication systems, if both systems are in a frequency division duplex (FDD) configuration [20]. If both systems are in a time division duplex configuration, ICSI can be obtained via exploiting channel reciprocity [20]. Regardless of the configuration of radars and communication systems, there is the incentive of zero interference, from radars, for communication systems if they collaborate in providing ICSI. Thus, we can safely assume the availability of ICSI for the sake of mitigating radar interference at communication systems.

III. FINITE ALPHABET CONSTANT-ENVELOPE BEAMPATTERN DESIGN

In this paper, we design QPSK waveforms having finite alphabets and constant-envelope property. We consider a uniform linear array (ULA) of M transmit antennas with inter-element spacing of half-wavelength. Then, the transmitted QPSK signal is given as

$$\tilde{\mathbf{x}}(n) = \begin{bmatrix} \tilde{x}_1(n) & \tilde{x}_2(n) & \cdots & \tilde{x}_M(n) \end{bmatrix}^T \quad (2)$$

where $\tilde{x}_m(n)$ is the QPSK signal from the m^{th} transmit element at time index n . Then, the received signal from a target at location θ_k is given as

$$\tilde{r}_k(n) = \sum_{m=1}^M e^{-j(m-1)\pi \sin \theta_k} \tilde{x}_m(n), \quad k = 1, 2, \dots, K, \quad (3)$$

where K is the total number of targets. We can write the received signal compactly as

$$\tilde{r}_k(n) = \mathbf{a}^H(\theta_k) \tilde{\mathbf{x}}(n) \quad (4)$$

where $\mathbf{a}(\theta_k)$ is the steering vector defined as

$$\mathbf{a}(\theta_k) = \begin{bmatrix} 1 & e^{-j\pi \sin \theta_k} & \cdots & e^{-j(M-1)\pi \sin \theta_k} \end{bmatrix}^T. \quad (5)$$

We can write the power received at the target located at θ_k as

$$\begin{aligned} P(\theta_k) &= \mathbb{E}\{\mathbf{a}^H(\theta_k) \tilde{\mathbf{x}}(n) \tilde{\mathbf{x}}^H(n) \mathbf{a}(\theta_k)\} \\ &= \mathbf{a}^H(\theta_k) \tilde{\mathbf{R}} \mathbf{a}(\theta_k) \end{aligned} \quad (6)$$

where $\tilde{\mathbf{R}}$ is correlation matrix of the transmitted QPSK waveform. The desired QPSK beampattern $\phi(\theta_k)$ is formed by minimizing the square of the error between $P(\theta_k)$ and $\phi(\theta_k)$ through a cost function defined as

$$J(\tilde{\mathbf{R}}) = \frac{1}{K} \sum_{k=1}^K \left(\mathbf{a}^H(\theta_k) \tilde{\mathbf{R}} \mathbf{a}(\theta_k) - \phi(\theta_k) \right)^2. \quad (7)$$

Since, $\tilde{\mathbf{R}}$ is covariance matrix of the transmitted signal it must be positive semi-definite. Moreover, due to the interest in constant-envelope property of waveforms, all antennas must transmit at the same power level. The optimization problem in equation (7) has some constraints and, thus, can't be chosen freely. In order to design finite alphabet constant-envelope waveforms, we must satisfy the following constraints:

$$\begin{aligned} C_1 : \mathbf{v}^H \tilde{\mathbf{R}} \mathbf{v} &\geq 0, & \forall \mathbf{v}, \\ C_2 : \tilde{\mathbf{R}}(m, m) &= c, & m = 1, 2, \dots, M, \end{aligned}$$

where C_1 satisfies the 'positive semi-definite' constraint and C_2 satisfies the 'constant-envelope' constraint. Thus, we have a constrained nonlinear optimization problem given as

$$\begin{aligned} \min_{\tilde{\mathbf{R}}} \quad & \frac{1}{K} \sum_{k=1}^K \left(\mathbf{a}^H(\theta_k) \tilde{\mathbf{R}} \mathbf{a}(\theta_k) - \phi(\theta_k) \right)^2 \\ \text{subject to} \quad & \mathbf{v}^H \tilde{\mathbf{R}} \mathbf{v} \geq 0, \quad \forall \mathbf{v}, \\ & \tilde{\mathbf{R}}(m, m) = c, \quad m = 1, 2, \dots, M. \end{aligned} \quad (8)$$

Ahmed et al. showed that, by using multi-dimensional spherical coordinates, this constrained nonlinear optimization can be transformed into an unconstrained nonlinear optimization [21]. Once $\tilde{\mathbf{R}}$ is synthesized, the waveform matrix $\tilde{\mathbf{X}}$ with N samples is given as

$$\tilde{\mathbf{X}} = \begin{bmatrix} \tilde{\mathbf{x}}(1) & \tilde{\mathbf{x}}(2) & \dots & \tilde{\mathbf{x}}(N) \end{bmatrix}^T. \quad (9)$$

This can be realized from

$$\tilde{\mathbf{X}} = \mathbf{X} \mathbf{\Lambda}^{1/2} \mathbf{W}^H \quad (10)$$

where $\mathbf{X} \in \mathbb{C}^{N \times M}$ is a matrix of zero mean and unit variance Gaussian random variables, $\mathbf{\Lambda} \in \mathbb{R}^{M \times M}$ is the diagonal matrix of eigenvalues, and $\mathbf{W} \in \mathbb{C}^{M \times M}$ is the matrix of eigenvectors of $\tilde{\mathbf{R}}$ [22]. Note that $\tilde{\mathbf{X}}$ has Gaussian distribution due to \mathbf{X} but the waveform produced is not guaranteed to have the CE property.

IV. FINITE ALPHABET CONSTANT-ENVELOPE QPSK WAVEFORMS

In [8], an algorithm to synthesize FACE QPSK waveforms to realize a given covariance matrix, $\tilde{\mathbf{R}}$, with complex entries was presented. However, it was not proved that such a covariance matrix is positive semi-definite and the constrained nonlinear optimization problem can be transformed into an un-constrained nonlinear optimization problem, we prove the claim in this paper.

Consider zero mean and unit variance Gaussian random variables (RVs) \tilde{x}_m and \tilde{y}_m that can be mapped onto a QPSK RV \tilde{z}_m through, as in [8],

$$\tilde{z}_m = \frac{1}{\sqrt{2}} \left[\text{sign}(\tilde{x}_m) + j \text{sign}(\tilde{y}_m) \right]. \quad (11)$$

Then, it is straight forward to write the (p, q) th element of the complex covariance matrix as

$$\mathbb{E}\{\tilde{z}_p \tilde{z}_q^*\} = \gamma_{pq} = \gamma_{\Re_{pq}} + j \gamma_{\Im_{pq}} \quad (12)$$

where $\gamma_{\Re_{pq}}$ and $\gamma_{\Im_{pq}}$ are the real and imaginary parts of γ_{pq} , respectively. If, Gaussian RVs $\tilde{x}_p, \tilde{x}_q, \tilde{y}_p$, and \tilde{y}_q are chosen such that

$$\begin{aligned}\mathbb{E}\{\tilde{x}_p\tilde{x}_q\} &= \mathbb{E}\{\tilde{y}_p\tilde{y}_q\} \\ \mathbb{E}\{\tilde{x}_p\tilde{y}_q\} &= -\mathbb{E}\{\tilde{y}_p\tilde{x}_q\}\end{aligned}\quad (13)$$

then we can write the real and imaginary parts of γ_{pq} as

$$\begin{aligned}\gamma_{\Re_{pq}} &= \mathbb{E}\left\{\text{sign}(\tilde{x}_p)\text{sign}(\tilde{x}_q)\right\} \\ \gamma_{\Im_{pq}} &= \mathbb{E}\left\{\text{sign}(\tilde{y}_p)\text{sign}(\tilde{x}_q)\right\}.\end{aligned}\quad (14)$$

Then, from equation (77) Appendix B, we have

$$\mathbb{E}\{\tilde{z}_p\tilde{z}_q\} = \frac{2}{\pi} \left[\sin^{-1} \left(\mathbb{E}\{\tilde{x}_p\tilde{x}_q\} \right) + j \sin^{-1} \left(\mathbb{E}\{\tilde{y}_p\tilde{x}_q\} \right) \right]. \quad (15)$$

The complex Gaussian covariance matrix $\tilde{\mathbf{R}}_g$ is defined as

$$\tilde{\mathbf{R}}_g \triangleq \Re(\mathbf{R}_g) + j \Im(\mathbf{R}_g) \quad (16)$$

where $\Re(\mathbf{R}_g)$ and $\Im(\mathbf{R}_g)$ both have real entries, since \mathbf{R}_g is a real Gaussian covariance matrix. Then, equation (15) can be written as

$$\tilde{\mathbf{R}} = \frac{2}{\pi} \left[\sin^{-1} \left(\Re(\mathbf{R}_g) \right) + j \sin^{-1} \left(\Im(\mathbf{R}_g) \right) \right]. \quad (17)$$

In [8], it is proposed to construct complex Gaussian covariance matrix via transform $\tilde{\mathbf{R}}_g = \tilde{\mathbf{U}}^H \tilde{\mathbf{U}}$, where $\tilde{\mathbf{U}}$ is given by equation (20). Then, $\tilde{\mathbf{U}}$ can be written as

$$\tilde{\mathbf{U}} = \Re(\tilde{\mathbf{U}}) + j \Im(\tilde{\mathbf{U}}) \quad (18)$$

where $\Re(\tilde{\mathbf{U}})$ and $\Im(\tilde{\mathbf{U}})$ are given by equations (21) and (22), respectively. Alternately, $\tilde{\mathbf{R}}_g$ can also be expressed as

$$\tilde{\mathbf{R}}_g = \left[\Re(\tilde{\mathbf{U}})^H \Re(\tilde{\mathbf{U}}) + \Im(\tilde{\mathbf{U}})^H \Im(\tilde{\mathbf{U}}) \right] + j \left[\Re(\tilde{\mathbf{U}})^H \Im(\tilde{\mathbf{U}}) - \Im(\tilde{\mathbf{U}})^H \Re(\tilde{\mathbf{U}}) \right]. \quad (19)$$

$$\tilde{\mathbf{U}} = \begin{pmatrix} e^{j\psi_1} & e^{j\psi_2} \sin(\psi_{21}) & e^{j\psi_3} \sin(\psi_{31}) \sin(\psi_{32}) & \cdots & e^{j\psi_M} \prod_{m=1}^{M-1} \sin(\psi_{Mm}) \\ 0 & e^{j\psi_2} \cos(\psi_{21}) & e^{j\psi_3} \sin(\psi_{31}) \cos(\psi_{32}) & \cdots & e^{j\psi_M} \prod_{m=1}^{M-2} \sin(\psi_{Mm}) \cos(\psi_{M,M-1}) \\ 0 & 0 & e^{j\psi_3} \cos(\psi_{31}) & \ddots & \vdots \\ \vdots & \vdots & \ddots & \cdots & e^{j\psi_M} \sin(\psi_{M1}) \cos(\psi_{M2}) \\ 0 & 0 & \cdots & \cdots & e^{j\psi_M} \cos(\psi_{M1}) \end{pmatrix} \quad (20)$$

$$\Re(\tilde{\mathbf{U}}) = \begin{pmatrix} \cos(\psi_1) & \cos(\psi_2) \sin(\psi_{21}) & \cos(\psi_3) \sin(\psi_{31}) \sin(\psi_{32}) & \cdots & \cos(\psi_M) \prod_{m=1}^{M-1} \sin(\psi_{Mm}) \\ 0 & \cos(\psi_2) \cos(\psi_{21}) & \cos(\psi_3) \sin(\psi_{31}) \cos(\psi_{32}) & \cdots & \cos(\psi_M) \prod_{m=1}^{M-2} \sin(\psi_{Mm}) \cos(\psi_{M,M-1}) \\ 0 & 0 & \cos(\psi_3) \cos(\psi_{31}) & \ddots & \vdots \\ \vdots & \vdots & \ddots & \cdots & \cos(\psi_M) \sin(\psi_{M1}) \cos(\psi_{M2}) \\ 0 & 0 & \cdots & \cdots & \cos(\psi_M) \cos(\psi_{M1}) \end{pmatrix} \quad (21)$$

$$\Im(\tilde{\mathbf{U}}) = \begin{pmatrix} \sin(\psi_1) & \sin(\psi_2) \sin(\psi_{21}) & \sin(\psi_3) \sin(\psi_{31}) \sin(\psi_{32}) & \cdots & \sin(\psi_M) \prod_{m=1}^{M-1} \sin(\psi_{Mm}) \\ 0 & \sin(\psi_2) \cos(\psi_{21}) & \sin(\psi_3) \sin(\psi_{31}) \cos(\psi_{32}) & \cdots & \sin(\psi_M) \prod_{m=1}^{M-2} \sin(\psi_{Mm}) \cos(\psi_{M,M-1}) \\ 0 & 0 & \sin(\psi_3) \cos(\psi_{31}) & \ddots & \vdots \\ \vdots & \vdots & \ddots & \cdots & \sin(\psi_M) \sin(\psi_{M1}) \cos(\psi_{M2}) \\ 0 & 0 & \cdots & \cdots & \sin(\psi_M) \cos(\psi_{M1}) \end{pmatrix} \quad (22)$$

Lemma 1. *If \mathbf{R}_g is a covariance matrix and*

$$\tilde{\mathbf{R}}_g = \Re(\mathbf{R}_g) + j \Im(\mathbf{R}_g) \quad (23)$$

then the complex covariance matrix $\tilde{\mathbf{R}}_g$ will always be positive semi-definite.

Proof: Please see Appendix C. ■

Lemma 1 satisfies constraint C_1 and $\tilde{\mathbf{R}}_g$ also satisfies constraint C_2 for $c = 1$. This helps to transform constrained nonlinear optimization into unconstrained nonlinear optimization in the following section.

In order to generate QPSK waveforms we define $N \times 2M$ matrix $\tilde{\mathbf{S}}$, of Gaussian RVs, as

$$\tilde{\mathbf{S}} \triangleq \begin{bmatrix} \tilde{\mathbf{X}} & \tilde{\mathbf{Y}} \end{bmatrix} \quad (24)$$

where $\tilde{\mathbf{X}}$ and $\tilde{\mathbf{Y}}$ are of each size $N \times M$, representing real and imaginary parts of QPSK waveform matrix, which is given as

$$\tilde{\mathbf{Z}} = \frac{1}{\sqrt{2}} \begin{bmatrix} \text{sign}(\tilde{\mathbf{X}}) + j \text{sign}(\tilde{\mathbf{Y}}) \end{bmatrix}. \quad (25)$$

The covariance matrix of $\tilde{\mathbf{S}}$ is given as

$$\tilde{\mathbf{R}}_{\tilde{\mathbf{S}}} = \mathbb{E}\{\tilde{\mathbf{S}}^H \tilde{\mathbf{S}}\} = \begin{bmatrix} \Re(\mathbf{R}_g) & \Im(\mathbf{R}_g) \\ -\Im(\mathbf{R}_g) & \Re(\mathbf{R}_g) \end{bmatrix}. \quad (26)$$

QPSK waveform matrix $\tilde{\mathbf{Z}}$ can be realized by the matrix $\tilde{\mathbf{S}}$ of Gaussian RVs which can be generated using equation (10) by utilizing $\tilde{\mathbf{R}}_{\tilde{\mathbf{S}}}$.

V. GAUSSIAN COVARIANCE MATRIX SYNTHESIS FOR DESIRED QPSK BEAMPATTERN

In this section, we prove that the desired QPSK beampattern can be directly synthesized by using the complex covariance matrix, $\tilde{\mathbf{R}}_g$, for complex Gaussian RVs. This generates M QPSK waveforms for the desired beampattern which satisfy the property of finite alphabet and constant-envelope. By exploiting the relationship between the complex Gaussian RVs and QPSK RVs we have

$$\tilde{\mathbf{R}} = \frac{2}{\pi} \left[\sin^{-1} \left(\Re(\mathbf{R}_g) \right) + j \sin^{-1} \left(\Im(\mathbf{R}_g) \right) \right]. \quad (27)$$

Lemma 2. *If $\tilde{\mathbf{R}}_g$ is a complex covariance matrix and*

$$\tilde{\mathbf{R}} = \frac{2}{\pi} \left[\sin^{-1} \left(\Re(\mathbf{R}_g) \right) + j \sin^{-1} \left(\Im(\mathbf{R}_g) \right) \right]$$

then $\tilde{\mathbf{R}}$ will always be positive semi-definite.

Proof: Please see Appendix C. ■

Using equation (27) we can rewrite the optimization problem in equation (8) as

$$\begin{aligned} \min_{\tilde{\mathbf{R}}} \quad & \frac{1}{K} \sum_{k=1}^K \left[\frac{2}{\pi} \mathbf{a}^H(\theta_k) \left\{ \sin^{-1} \left(\Re(\mathbf{R}_g) \right) + j \sin^{-1} \left(\Im(\mathbf{R}_g) \right) \right\} \mathbf{a}(\theta_k) - \phi(\theta_k) \right]^2 \\ \text{subject to} \quad & \mathbf{v}^H \tilde{\mathbf{R}} \mathbf{v} \geq 0, \quad \forall \mathbf{v}, \\ & \tilde{\mathbf{R}}(m, m) = c, \quad m = 1, 2, \dots, M. \end{aligned} \quad (28)$$

$$\begin{aligned} J(\Theta) = \frac{1}{K} \sum_{k=1}^K \left[\frac{2}{\pi} \mathbf{a}^H(\theta_k) \left\{ \sin^{-1} \left(\Re(\tilde{\mathbf{U}})^H \Re(\tilde{\mathbf{U}}) + \Im(\tilde{\mathbf{U}})^H \Im(\tilde{\mathbf{U}}) \right) \right. \right. \\ \left. \left. + j \sin^{-1} \left(\Re(\tilde{\mathbf{U}})^H \Im(\tilde{\mathbf{U}}) - \Im(\tilde{\mathbf{U}})^H \Re(\tilde{\mathbf{U}}) \right) \right\} \mathbf{a}^H(\theta_k) - \alpha \phi(\theta_k) \right]^2 \end{aligned} \quad (29)$$

Since, the matrix $\tilde{\mathbf{U}}$ is already known, we can formulate $\tilde{\mathbf{R}}_g$ via equation (19). We can also write the (p, q) th element of the upper triangular matrix $\tilde{\mathbf{R}}_g$ by first writing the (p, q) th element of the upper triangular matrix $\Re(\mathbf{R}_g(p, q))$ as

$$\Re(\mathbf{R}_g(p, q)) = \begin{cases} \prod_{l=1}^{q-1} \sin(\Psi_{ql}) \prod_{s=1}^p \prod_{u=1}^q f(s, u), & p > q \\ 1, & p = q \end{cases} \quad (30)$$

where $f(s, u) = \cos(\Psi_s) \cos(\Psi_u) + \sin(\Psi_s) \sin(\Psi_u)$; and the (p, q) th element of the upper triangular matrix $\Im(\mathbf{R}_g(p, q))$ as

$$\Im(\mathbf{R}_g(p, q)) = \begin{cases} g(p, q) \prod_{l=1}^{q-1} \sin(\Psi_{ql}), & p > q \\ 0, & p = q \end{cases} \quad (31)$$

where $g(p, q) = \cos(\Psi_p) \sin(\Psi_q) + \sin(\Psi_p) \cos(\Psi_q)$. Thus, we can write the (p, q) th element of the upper triangular matrix $\tilde{\mathbf{R}}_g$ as

$$\tilde{\mathbf{R}}_g(p, q) = \begin{cases} \Re(\mathbf{R}_g(p, q)) + j\Im(\mathbf{R}_g(p, q)), & p > q \\ 1, & p = q. \end{cases} \quad (32)$$

By utilizing the information of $\tilde{\mathbf{U}}$, the constrained optimization problem in equation (28) can be transformed into an unconstrained optimization problem that can be written as equation (29), where

$$\Theta = \begin{bmatrix} \Psi^T & \tilde{\Psi}^T & \alpha \end{bmatrix}^T, \quad (33)$$

and

$$\Psi^T = \begin{bmatrix} \Psi_{21} & \Psi_{21} & \cdots & \Psi_{21} \end{bmatrix}^T, \\ \tilde{\Psi}^T = \begin{bmatrix} \Psi_1 & \Psi_2 & \cdots & \Psi_M \end{bmatrix}^T.$$

The optimization is over $M(M-1)/2 + M$ elements Ψ_{mn} and Ψ_l . The advantage of this approach lies in the free selection of elements of Θ without effecting the positive semi-definite property and diagonal elements of $\tilde{\mathbf{R}}_g$. Noting that $\tilde{\mathbf{U}}$ and $\tilde{\mathbf{R}}_g$ are functions of Θ , we can alternately write the cost-function, in equation (29), as

$$J(\Theta) = \frac{1}{K} \sum_{k=1}^K \left[\frac{2}{\pi} \mathbf{a}^H(\theta_k) \sin^{-1} \left(\Re(\mathbf{R}_g) \right) \mathbf{a}(\theta_k) + \frac{2j}{\pi} \mathbf{a}^H(\theta_k) \sin^{-1} \left(\Im(\mathbf{R}_g) \right) \mathbf{a}(\theta_k) - \alpha \phi(\theta_k) \right]^2. \quad (34)$$

First, the partial differentiation of $J(\Theta)$ with respect to any element of Ψ , say Ψ_{mn} , can be found as

$$\frac{\partial J(\Theta)}{\partial \Psi_{mn}} = \left[\frac{2}{K} \sum_{k=1}^K \left\{ \frac{2}{\pi} \mathbf{a}^H(\theta_k) \sin^{-1} \left(\Re(\mathbf{R}_g) \right) \mathbf{a}(\theta_k) + \frac{2j}{\pi} \mathbf{a}^H(\theta_k) \sin^{-1} \left(\Im(\mathbf{R}_g) \right) \mathbf{a}(\theta_k) - \alpha \phi(\theta_k) \right\} \right] \\ \times \left[\frac{\partial}{\partial \Psi_{mn}} \left\{ \frac{2}{\pi} \mathbf{a}^H(\theta_k) \sin^{-1} \left(\Re(\mathbf{R}_g) \right) \mathbf{a}(\theta_k) + \frac{2j}{\pi} \mathbf{a}^H(\theta_k) \sin^{-1} \left(\Im(\mathbf{R}_g) \right) \mathbf{a}(\theta_k) \right\} \right]. \quad (35)$$

The matrix $\Re(\mathbf{R}_g)$ is real and symmetric, i.e., $\Re(\mathbf{R}_g(p, q)) = \Re(\mathbf{R}_g(q, p))$, at the same time, $\Im(\mathbf{R}_g)$ has real entries but is skew-symmetric, i.e., $\Im(\mathbf{R}_g(p, q)) = -\Im(\mathbf{R}_g(q, p))$. These observations enables us to write equation (35) in a simpler form

$$\frac{\partial J(\Theta)}{\partial \Psi_{mn}} = \left[\frac{4}{K} \sum_{k=1}^K \left\{ \frac{2}{\pi} \mathbf{a}^H(\theta_k) \sin^{-1} \left(\Re(\mathbf{R}_g) \right) \mathbf{a}(\theta_k) + \frac{2j}{\pi} \mathbf{a}^H(\theta_k) \sin^{-1} \left(\Im(\mathbf{R}_g) \right) \mathbf{a}(\theta_k) - \alpha \phi(\theta_k) \right\} \right] \\ \times \left[\frac{2}{\pi} \sum_{p=1}^{M-1} \sum_{q=p+1}^M \frac{\cos(\pi|p-q|\sin(\theta_k))}{\sqrt{1 - \Re(\mathbf{R}_g^2(p, q))}} \frac{\partial \Re(\mathbf{R}_g(p, q))}{\partial \Psi_{mn}} \right]. \quad (36)$$

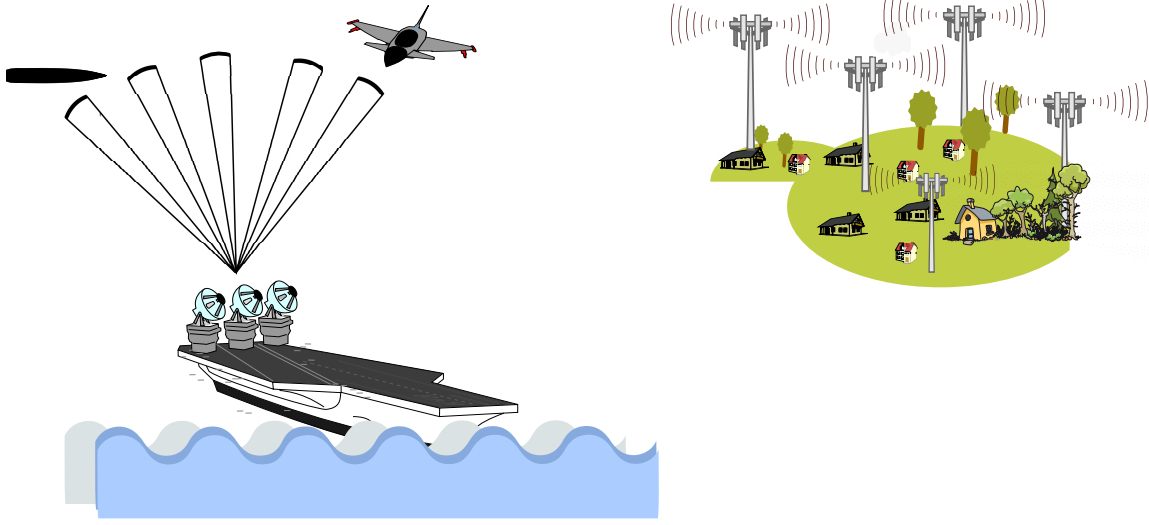


Fig. 1. Spectrum Sharing Scenario: Seaborne MIMO radar sharing spectrum with a cellular system.

Moreover, $\Re(\mathbf{R}_g)$ contains only $(M - 1)$ terms which depend on Ψ_{mn} , thus, equation (36) further simplifies as

$$\begin{aligned} \frac{\partial J(\Theta)}{\partial \Psi_{mn}} &= \frac{8}{\pi K} \left[\sum_{k=1}^K \left\{ \frac{2}{\pi} \mathbf{a}^H(\theta_k) \sin^{-1}(\Re(\mathbf{R}_g)) \mathbf{a}(\theta_k) + \frac{2J}{\pi} \mathbf{a}^H(\theta_k) \sin^{-1}(\Im(\mathbf{R}_g)) \mathbf{a}(\theta_k) - \alpha \phi(\theta_k) \right\} \right] \\ &\times \left[\left\{ \sum_{p=1}^{m-1} \frac{\cos(\pi|p-m|\sin(\theta_k))}{\sqrt{1-\Re(\mathbf{R}_g^2(p,m))}} \frac{\partial \Re(\mathbf{R}_g(p,m))}{\partial \Psi_{mn}} + \sum_{q=m+1}^M \frac{\cos(\pi|m-q|\sin(\theta_k))}{\sqrt{1-\Re(\mathbf{R}_g^2(m,q))}} \frac{\partial \Re(\mathbf{R}_g(m,q))}{\partial \Psi_{mn}} \right\} \right]. \end{aligned} \quad (37)$$

Second, the partial differentiation of $J(\Theta)$ with respect to any element of $\tilde{\Psi}$, say Ψ_l , can be found in the same manner as was found for Ψ_{mn} , i.e.,

$$\begin{aligned} \frac{\partial J(\Theta)}{\partial \Psi_l} &= \frac{8}{\pi K} \left[\sum_{k=1}^K \left\{ \frac{2}{\pi} \mathbf{a}^H(\theta_k) \sin^{-1}(\Re(\mathbf{R}_g)) \mathbf{a}(\theta_k) + \frac{2J}{\pi} \mathbf{a}^H(\theta_k) \sin^{-1}(\Im(\mathbf{R}_g)) \mathbf{a}(\theta_k) - \alpha \phi(\theta_k) \right\} \right] \\ &\times \left[\sum_{p=1}^{M-1} \sum_{q=p+1}^M \frac{\cos(\pi|p-q|\sin(\theta_k))}{\sqrt{1-\Re(\mathbf{R}_g^2(p,q))}} \frac{\partial \Re(\mathbf{R}_g(p,q))}{\partial \Psi_l} \right]. \end{aligned} \quad (38)$$

Finally, the partial differentiation of $J(\Theta)$ with respect to α is

$$\frac{\partial J(\Theta)}{\partial \alpha} = \frac{-2\phi(\theta_k)}{K} \left[\sum_{k=1}^K \left\{ \frac{2}{\pi} \mathbf{a}^H(\theta_k) \sin^{-1}(\Re(\mathbf{R}_g)) \mathbf{a}(\theta_k) + \frac{2J}{\pi} \mathbf{a}^H(\theta_k) \sin^{-1}(\Im(\mathbf{R}_g)) \mathbf{a}(\theta_k) - \alpha \phi(\theta_k) \right\} \right]. \quad (39)$$

VI. RADAR-CELLULAR SYSTEM SPECTRUM SHARING

In the following sections, we will discuss our spectrum sharing architecture and spectrum sharing algorithms for the 3550-3650 MHz band under consideration, which is co-shared by MIMO radar and cellular systems. .

A. Architecture

Considering the coexistence scenario in Fig. 1, where the radar is sharing \mathcal{K} interference channels with the cellular system, the received signal at the i^{th} BS can be written as

$$\mathbf{y}_i(n) = \mathbf{H}_i \tilde{\mathbf{x}}(n) + \sum_j \mathbf{H}_{i,j} \mathbf{s}_j(n) + \mathbf{w}(n) \quad (40)$$

In order to avoid interference to the i^{th} BS, the radar shapes its waveform $\tilde{\mathbf{x}}(n)$ such that it is in the null-space of \mathbf{H}_i , i.e. $\mathbf{H}_i \tilde{\mathbf{x}}(n) = \mathbf{0}$.

B. Projection Matrix

In this section, we formulate a projection algorithm to project the radar signal onto the null space of interference channel \mathbf{H}_i . Assuming, the MIMO radar has ICSI for all \mathbf{H}_i interference channels, either through feedback or channel reciprocity, we can perform a singular value decomposition (SVD) to find the null space of \mathbf{H}_i and use it to construct a projector matrix. First, we find SVD of \mathbf{H}_i , i.e.,

$$\mathbf{H}_i = \mathbf{U}_i \mathbf{\Sigma}_i \mathbf{V}_i^H. \quad (41)$$

Now, let us define

$$\tilde{\mathbf{\Sigma}}_i \triangleq \text{diag}(\tilde{\sigma}_{i,1}, \tilde{\sigma}_{i,2}, \dots, \tilde{\sigma}_{i,p}) \quad (42)$$

where $p \triangleq \min(N^{\text{BS}}, M)$ and $\tilde{\sigma}_{i,1} > \tilde{\sigma}_{i,2} > \dots > \tilde{\sigma}_{i,q} > \tilde{\sigma}_{i,q+1} = \tilde{\sigma}_{i,q+2} = \dots = \tilde{\sigma}_{i,p} = 0$. Next, we define

$$\tilde{\mathbf{\Sigma}}'_i \triangleq \text{diag}(\tilde{\sigma}'_{i,1}, \tilde{\sigma}'_{i,2}, \dots, \tilde{\sigma}'_{i,M}) \quad (43)$$

where

$$\tilde{\sigma}'_{i,u} \triangleq \begin{cases} 0, & \text{for } u \leq q, \\ 1, & \text{for } u > q. \end{cases} \quad (44)$$

Using above definitions we can now define our projection matrix, i.e.,

$$\mathbf{P}_i \triangleq \mathbf{V}_i \tilde{\mathbf{\Sigma}}'_i \mathbf{V}_i^H. \quad (45)$$

Below, we show two properties of projection matrices showing that \mathbf{P}_i is a valid projection matrix.

Property 1. $\mathbf{P}_i \in \mathbb{C}^{M \times M}$ is a projection matrix if and only if $\mathbf{P}_i = \mathbf{P}_i^H = \mathbf{P}_i^2$.

Proof: Let's start by showing the 'only if' part. First, we show $\mathbf{P}_i = \mathbf{P}_i^H$. Taking Hermitian of equation (45) we have

$$\mathbf{P}_i^H = (\mathbf{V}_i \tilde{\mathbf{\Sigma}}'_i \mathbf{V}_i^H)^H = \mathbf{P}_i. \quad (46)$$

Now, squaring equation (45) we have

$$\mathbf{P}_i^2 = \mathbf{V}_i \tilde{\mathbf{\Sigma}}_i \mathbf{V}_i^H \times \mathbf{V}_i \tilde{\mathbf{\Sigma}}_i \mathbf{V}_i^H = \mathbf{P}_i \quad (47)$$

where above equation follows from $\mathbf{V}^H \mathbf{V}_i = \mathbf{I}$ (since they are orthonormal matrices) and $(\tilde{\Sigma}'_i)^2 = \tilde{\Sigma}'_i$ (by construction). From equations (46) and (47) it follows that $\mathbf{P}_i = \mathbf{P}_i^H = \mathbf{P}_i^2$. Next, we show \mathbf{P}_i is a projector by showing that if $\mathbf{v} \in \text{range}(\mathbf{P}_i)$, then $\mathbf{P}_i \mathbf{v} = \mathbf{v}$, i.e., for some \mathbf{w} , $\mathbf{v} = \mathbf{P}_i \mathbf{w}$, then

$$\mathbf{P}_i \mathbf{v} = \mathbf{P}_i(\mathbf{P}_i \mathbf{w}) = \mathbf{P}_i^2 \mathbf{w} = \mathbf{P}_i \mathbf{w} = \mathbf{v}. \quad (48)$$

Moreover, $\mathbf{P}_i \mathbf{v} - \mathbf{v} \in \text{null}(\mathbf{P}_i)$, i.e.,

$$\mathbf{P}_i(\mathbf{P}_i \mathbf{v} - \mathbf{v}) = \mathbf{P}_i^2 \mathbf{v} - \mathbf{P}_i \mathbf{v} = \mathbf{P}_i \mathbf{v} - \mathbf{P}_i \mathbf{v} = \mathbf{0}. \quad (49)$$

This concludes our proof. ■

Property 2. $\mathbf{P}_i \in \mathbb{C}^{M \times M}$ is an orthogonal projection matrix onto the null space of $\mathbf{H}_i \in \mathbb{C}^{N^{BS} \times M}$

Proof: Since $\mathbf{P}_i = \mathbf{P}_i^H$, we can write

$$\mathbf{H}_i \mathbf{P}_i^H = \mathbf{U}_i \tilde{\Sigma}_i \mathbf{V}_i^H \times \mathbf{V}_i \tilde{\Sigma}'_i \mathbf{V}_i^H = \mathbf{0}. \quad (50)$$

The above results follows from noting that $\tilde{\Sigma}_i \tilde{\Sigma}'_i = \mathbf{0}$ by construction. ■

The formation of projection matrix in the waveform design process is presented in the form of Algorithm 1.

Algorithm 1 Projection Algorithm

if \mathbf{H}_i received from waveform design algorithm **then**

 Perform SVD on \mathbf{H}_i (i.e. $\mathbf{H}_i = \mathbf{U}_i \Sigma_i \mathbf{V}_i^H$)

 Construct $\tilde{\Sigma}_i = \text{diag}(\tilde{\sigma}_{i,1}, \tilde{\sigma}_{i,2}, \dots, \tilde{\sigma}_{i,p})$

 Construct $\tilde{\Sigma}'_i = \text{diag}(\tilde{\sigma}'_{i,1}, \tilde{\sigma}'_{i,2}, \dots, \tilde{\sigma}'_{i,M})$

 Setup projection matrix $\mathbf{P}_i = \mathbf{V}_i \tilde{\Sigma}'_i \mathbf{V}_i^H$.

 Send \mathbf{P}_i to waveform design algorithm.

end if

VII. WAVEFORM DESIGN FOR SPECTRUM SHARING

In the previous section, we designed finite alphabet constant-envelope QPSK waveforms by solving a beampattern matching optimization problem. In this section, we extend the beampattern matching optimization problem and introduce new constraints in order to tailor waveforms that don't cause interference to communication systems when MIMO radar and communication systems are sharing spectrum. We design spectrum sharing waveforms for two cases: the first case is for a stationary maritime MIMO radar and the second case is for moving maritime MIMO radar. The waveform design in these contexts is and its performance is discussed in the next sections.

A. Stationary maritime MIMO radar

Consider a naval ship docked at the harbor. The radar mounted on top of that ship is also stationary. The interference channels are also stationary due to non-movement of ship and BSs. In such a scenario, the CSI has little to no variations and thus it is feasible to include the constraint of NSP, equation (52), into the optimization problem. Thus, the new optimization problem is formulated as

$$\min_{\psi_{ij}, \psi_l} \frac{1}{K} \sum_{k=1}^K \left[\frac{2}{\pi} \mathbf{a}^H(\theta_k) \mathbf{P}_i \left\{ \sin^{-1} \left(\Re(\tilde{\mathbf{U}})^H \Re(\tilde{\mathbf{U}}) + \Im(\tilde{\mathbf{U}})^H \Im(\tilde{\mathbf{U}}) \right) + j \sin^{-1} \left(\Re(\tilde{\mathbf{U}})^H \Im(\tilde{\mathbf{U}}) - \Im(\tilde{\mathbf{U}})^H \Re(\tilde{\mathbf{U}}) \right) \right\} \right. \\ \left. \times \mathbf{P}_i^H \mathbf{a}^H(\theta_k) - \alpha \phi(\theta_k) \right]^2. \quad (51)$$

A drawback of this approach is that it does not guarantee to generate constant-envelope radar waveform. However, the designed waveform is in the null space of the interference channel, thus, satisfying spectrum sharing constraints. The waveform generation process is shown using the block diagram of Figure 2. Note that, \mathcal{K} waveforms are designed, as we have \mathcal{K} interference channels that are static. Using the projection matrix \mathbf{P}_i , the NSP projected waveform can be obtained as

$$\tilde{\mathbf{Z}}_{\text{NSP}}^{\text{opt}} = \tilde{\mathbf{Z}}_i^{\text{opt}} \mathbf{P}_i^H. \quad (52)$$

The correlation matrix of the NSP waveform is given as

$$\check{\mathbf{R}}_i = \frac{1}{N} \left(\tilde{\mathbf{Z}}_{\text{NSP}}^{\text{opt}} \right)^H \tilde{\mathbf{Z}}_{\text{NSP}}^{\text{opt}}. \quad (53)$$

We propose to select the transmitted waveform with covariance matrix $\check{\mathbf{R}}_i$ is as close as possible to the desired covariance matrix, i.e.,

$$i_{\min} \triangleq \arg \min_{1 \leq i \leq \mathcal{K}} \left[\frac{1}{K} \sum_{k=1}^K \left(\mathbf{a}^H(\theta_k) \check{\mathbf{R}}_i \mathbf{a}(\theta_k) - \phi(\theta_k) \right)^2 \right] \quad (54)$$

$$\tilde{\mathbf{R}}_{\text{NSP}}^{\text{opt}} \triangleq \check{\mathbf{R}}_{i_{\min}}. \quad (55)$$

Equivalently, we select \mathbf{P}_i which projects maximum power at target locations. Thus, for stationary MIMO radar waveform with spectrum sharing constraints we propose Algorithm (2).

B. Moving maritime MIMO radar

Consider the case of a moving naval ship. The radar mounted on top of the ship is also moving, thus, the interference channels are varying due to the motion of ship. Due to time-varying ICSI, it is not feasible to include the NSP in the optimization problem. For this case, we first design finite alphabet constant-envelope QPSK waveforms, using the optimization problem in equation (29), and then use NSP to satisfy spectrum sharing constraints using transform

$$\check{\mathbf{Z}}_i = \tilde{\mathbf{Z}} \mathbf{P}_i^H. \quad (56)$$

The waveform generation process is shown using the block diagram of Figure 3. Note that only one waveform is designed using the optimization problem in equation (29) but \mathcal{K} projection operations are performed via equation

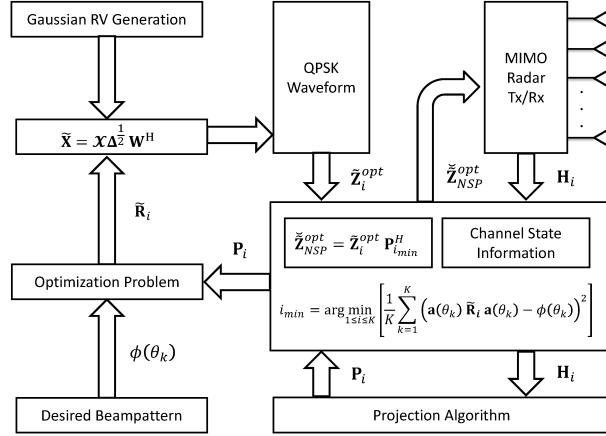


Fig. 2. Block diagram of waveform generation process for a stationary MIMO radar with spectrum sharing constraints.

Algorithm 2 Stationary MIMO Radar Waveform Design Algorithm with Spectrum Sharing Constraints

loop

for $i = 1 : \mathcal{K}$ **do**

Get CSI of \mathbf{H}_i through feedback from the i^{th} BS.

Send \mathbf{H}_i to Algorithm (1) for the formation of projection matrix \mathbf{P}_i .

Receive the i^{th} projection matrix \mathbf{P}_i from Algorithm (1).

Design QPSK waveform $\tilde{\mathbf{Z}}_i^{\text{opt}}$ using the optimization problem in equation (51).

Project the QPSK waveform onto the null space of i^{th} interference channel using $\tilde{\mathbf{Z}}_{\text{NSP}}^{\text{opt}} = \tilde{\mathbf{Z}}_i^{\text{opt}} \mathbf{P}_i^H$.

end for

Find $i_{\min} = \arg \min_{1 \leq i \leq \mathcal{K}} \left[\frac{1}{K} \sum_{k=1}^K \left(\mathbf{a}^H(\theta_k) \tilde{\mathbf{R}}_i \mathbf{a}(\theta_k) - \phi(\theta_k) \right)^2 \right]$.

Set $\tilde{\mathbf{R}}_{\text{NSP}}^{\text{opt}} = \tilde{\mathbf{R}}_{i_{\min}}$ as the covariance matrix of the desired NSP QPSK waveforms to be transmitted.

end loop

(56). The transmitted waveform is selected on the basis of minimum Forbenius norm with respect to the designed waveform using the optimization problem in equation (29), i.e.,

$$i_{\min} \triangleq \arg \min_{1 \leq i \leq \mathcal{K}} \|\tilde{\mathbf{Z}} \mathbf{P}_i^H - \tilde{\mathbf{Z}}\|_F \quad (57)$$

$$\tilde{\mathbf{Z}}_{\text{NSP}} \triangleq \tilde{\mathbf{Z}}_{i_{\min}}. \quad (58)$$

The correlation matrix of this transmitted waveform is given as

$$\tilde{\mathbf{R}}_{\text{NSP}} = \frac{1}{N} \tilde{\mathbf{Z}}_{\text{NSP}}^H \tilde{\mathbf{Z}}_{\text{NSP}}. \quad (59)$$

Thus, for moving MIMO radar waveform with spectrum sharing constraints we propose Algorithm (3).

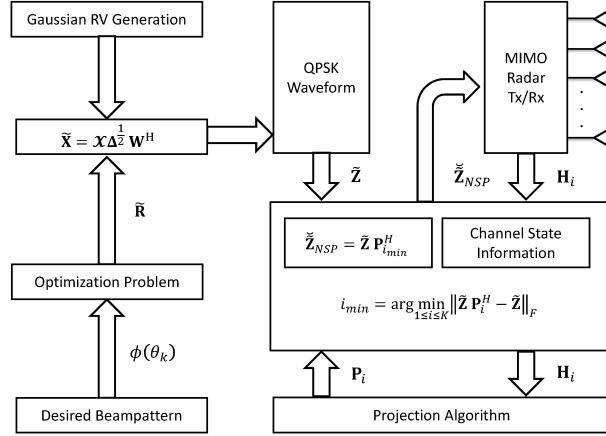


Fig. 3. Block diagram of waveform generation process for a moving MIMO radar with spectrum sharing constraints.

Algorithm 3 Moving MIMO Radar Waveform Design Algorithm with Spectrum Sharing Constraints

Design FACE QPSK waveform $\tilde{\mathbf{Z}}$ using the optimization problem in equation (29).

loop

for $i = 1 : \mathcal{K}$ **do**

Get CSI of \mathbf{H}_i through feedback from the i^{th} BS.

Send \mathbf{H}_i to Algorithm (1) for the formation of projection matrix \mathbf{P}_i .

Receive the i^{th} projection matrix \mathbf{P}_i from Algorithm (1).

Project the FACE QPSK waveform onto the null space of i^{th} interference channel using $\tilde{\mathbf{Z}}_i = \tilde{\mathbf{Z}}\mathbf{P}_i^H$.

end for

Find $i_{\min} = \arg \min_{1 \leq i \leq \mathcal{K}} \|\tilde{\mathbf{Z}}\mathbf{P}_i^H - \tilde{\mathbf{Z}}\|_F$.

Set $\tilde{\mathbf{R}}_{\text{NSP}}$ as the covariance matrix of the desired NSP QPSK waveforms to be transmitted.

end loop

VIII. SIMULATION

In order to design QPSK waveforms with spectrum sharing constraints, we use a uniform linear array (ULA) of ten elements, i.e., $M = 10$, with an inter-element spacing of half-wavelength. Each antenna transmits waveform with unit power and $N = 100$ symbols. We average the resulting beampattern over 100 Monte-Carlo trials of QPSK waveforms. At each run of Monte Carlo simulation we generate a Rayleigh interference channel with dimensions $N_{\text{BS}} \times M$, calculate its null space, and solve the optimization problem for stationary and moving maritime MIMO radar.

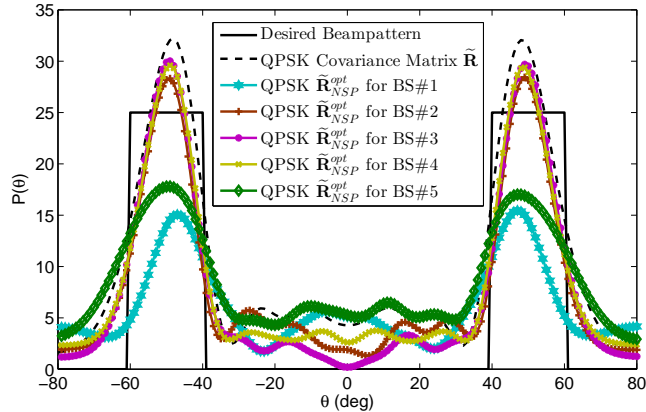


Fig. 4. QPSK waveform for stationary MIMO radar, sharing RF environment with five BSs each equipped with *three* antennas.

A. Waveform for stationary radar

In this section, we design the transmit beampattern for a stationary MIMO radar. The desired beampattern has two main lobes from -60° to -40° and from 40° to 60° . The QPSK transmit beampattern for stationary maritime MIMO radar is obtained by solving the optimization problem in equation (51). We give different examples to cover various scenarios involving different number of BSs and different configuration of MIMO antennas at the BSs. We also give one example to demonstrate the efficacy of Algorithms (1) and (2) in BS selection and its impact on the waveform design problem.

Example 1: Cellular System with five BSs and $\{3, 5, 7\}$ MIMO antennas and stationary MIMO radar

In this example, we design waveform for a stationary MIMO radar in the presence of a cellular system with five BSs. We look at three cases where we vary the number of BS antennas from $\{3, 5, 7\}$. In Figure 4, we show the designed waveforms for all five BSs each equipped with 3 MIMO antennas. Note that, due to channel variations there is a large variation in the amount of power projected onto target locations for different BSs. But for certain BSs, the projected waveform is close to the desired waveform. In Figure 5, we show the designed waveforms for all five BSs each equipped with 5 MIMO antennas. Similar to the previous case, due to channel variations there is a large variation in the amount of power projected onto target locations for different BSs. However, the power projected onto the target is less when compared with the previous case. We increase the number of antennas to 7 in Figure 6, and notice that the amount of power projected onto the targets is least as compared to previous two cases. This is because when $N_{BS} \ll M$ we have a larger null space to project radar waveform and this results in the projected waveform closer to the desired waveform. However, when $N_{BS} < M$, this is not the case.

Example 2: Performance of Algorithms (1) and (2) in BS selection for spectrum sharing with stationary MIMO radar

In Examples 1, we designed waveforms for different number of BSs with different antenna configurations. As we showed, for some BSs the designed waveform was close to the desired waveform but for other it wasn't and the

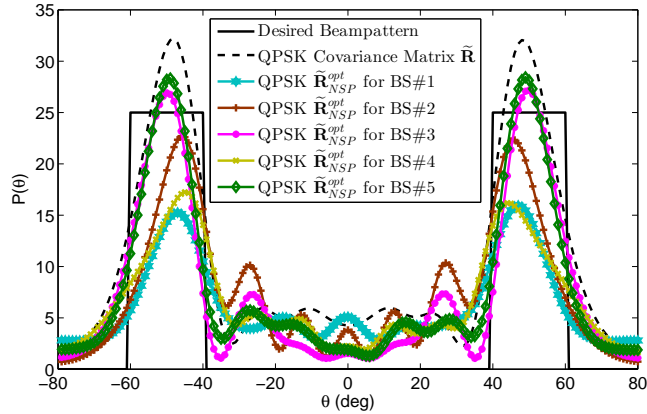


Fig. 5. QPSK waveform for stationary MIMO radar, sharing RF environment with five BSs each equipped with *five* antennas.

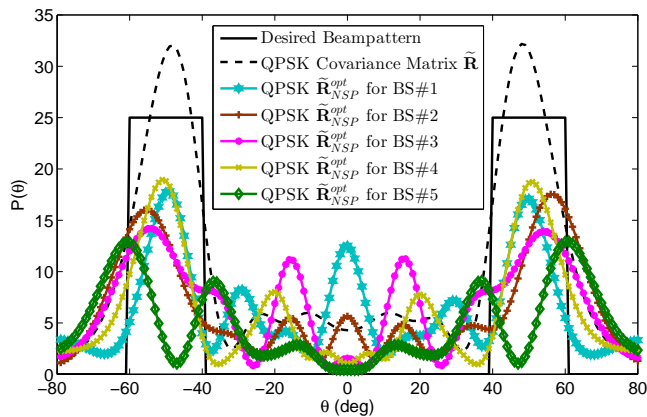


Fig. 6. QPSK waveform for stationary MIMO radar, sharing RF environment with five BSs each equipped with *seven* antennas.

projected waveform was closer to the desired waveform when $N_{\text{BS}} \ll M$ than when $N_{\text{BS}} < M$. In Figure 7, we use Algorithms (1) and (2) to select the waveform which projects maximum power on the targets or equivalently the projected waveform is closest to the desired waveform. We apply Algorithms (1) and (2) to the cases when $N_{\text{BS}} = \{3, 5, 7\}$ and select the waveform which projects maximum power on the targets. It can be seen that Algorithm (2) helps us to select waveform for stationary MIMO radar which results in best performance for radar in terms of projected waveform as close as possible to the desired waveform in addition of meeting spectrum sharing constraints.

B. Waveform for moving radar

In this section, we design transmit beampattern for a moving MIMO radar. The desired beampattern has two main lobes from -60° to -40° and from 40° to 60° . The QPSK transmit beampattern for moving maritime MIMO

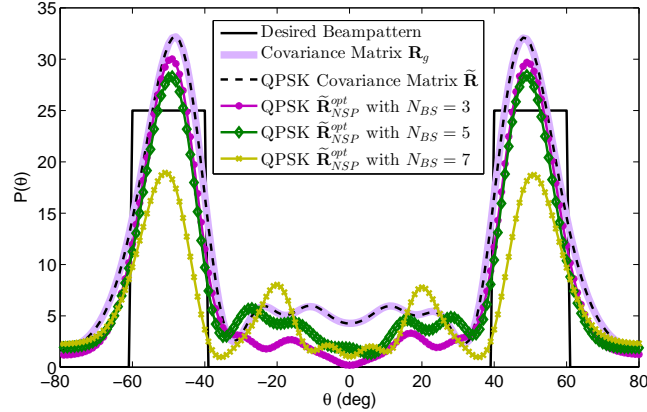


Fig. 7. Algorithm (2) is used to select the waveform which projects maximum power on the targets when $N_{BS} = \{3, 5, 7\}$ in the presence of five BSs.

radar is obtained by solving the optimization problem in equation (34) and then projecting the resulting waveform onto the null space of \mathbf{H}_i using the projection matrix in equation (56). We give different examples to cover various scenarios involving different number of BSs and different configuration of MIMO antennas at the BSs. We also give one example to demonstrate the efficacy of Algorithms (1) and (3) in BS selection and its impact on the waveform design problem.

Example 3: Cellular System with five BSs each with $\{3, 5, 7\}$ MIMO antennas and moving MIMO radar

In this example, we design waveform for a moving MIMO radar in the presence of a cellular system with five BSs. We look at three cases where we vary the number of BS antennas from $\{3, 5, 7\}$. In Figure 8, we show the designed waveforms for all five BSs each equipped with 3 MIMO antennas. Note that, due to channel variations there is a large variation in the amount of power projected onto target locations for different BSs. When compared with Figure 4, the power projected onto the target by NSP waveform is less due to the mobility of radar. In Figure 9, we show the designed waveforms for all five BSs each equipped with 5 MIMO antennas. Similar to the previous case, due to channel variations there is a large variation in the amount of power projected onto target locations for different BSs. However, the power projected onto the target is less when compared with the previous case. We increase the number of antennas to 7 in Figure 10, and notice that the amount of power projected onto the targets is least as compared to previous two cases. This is because when $N_{BS} \ll M$ we have a larger null space to project radar waveform and this results in the projected waveform closer to the desired waveform. However, when $N_{BS} < M$, this is not the case. Moreover, due to mobility of the radar, the amount of power projected for all three cases considered in this example are less than the similar example considered for stationary radar.

Example 4: Performance of Algorithms (1) and (3) in BS selection for spectrum sharing with moving MIMO radar

In Examples 3, we designed waveforms for different number of BSs with different antenna configurations. As we

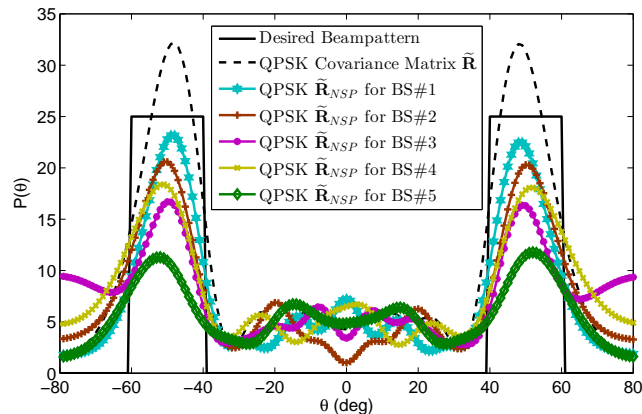


Fig. 8. QPSK waveform for moving MIMO radar, sharing RF environment with five BSs each equipped with *three* antennas.

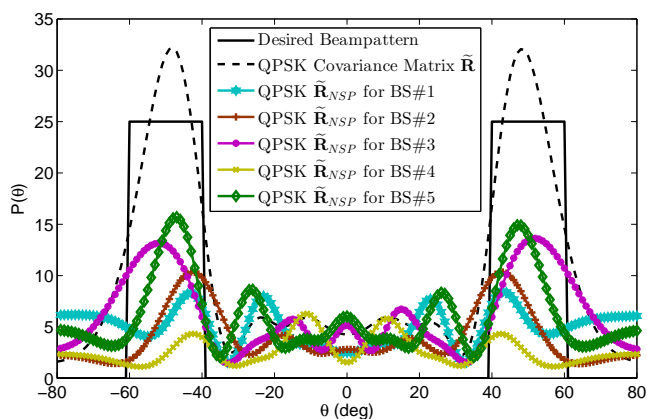


Fig. 9. QPSK waveform for moving MIMO radar, sharing RF environment with five BSs each equipped with *five* antennas.

showed, for some BSs the designed waveform was close to the desired waveform but for other it wasn't and the projected waveform was closer to the desired waveform when $N_{BS} \ll M$ than when $N_{BS} < M$. In Figure 11, we use Algorithms (1) and (3) to select the waveform which has the least Forbenius norm with respect to the designed waveform. We apply Algorithms (1) and (3) to the cases when $N_{BS} = \{3, 5, 7\}$ and select the waveform which has minimum Forbenius norm. It can be seen that Algorithm (3) helps us to select waveform for stationary MIMO radar which results in best performance for radar in terms of projected waveform as close as possible to the desired waveform in addition of meeting spectrum sharing constraints.

IX. CONCLUSION

Waveform design for MIMO radar is an active topic of research in the signal processing community. This work addressed the problem of designing MIMO radar waveforms with constant-envelope, which are very desirable from

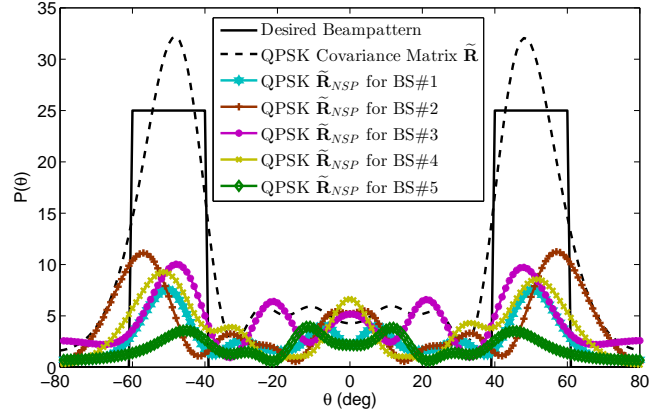


Fig. 10. QPSK waveform for moving MIMO radar, sharing RF environment with five BSs each equipped with *seven* antennas.

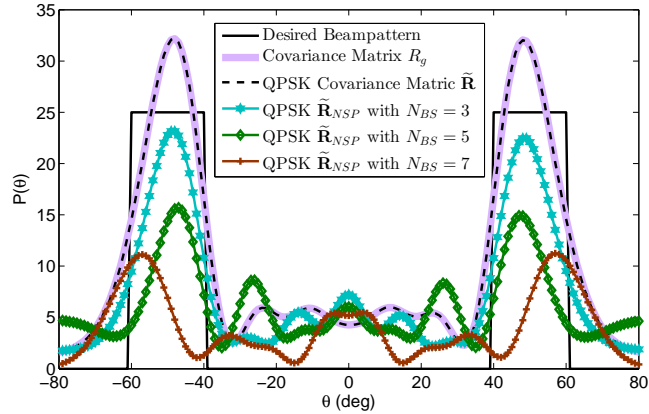


Fig. 11. Algorithm (3) is used to select the waveform which projects maximum power on the targets when $N_{BS} = \{3, 5, 7\}$ in the presence of five BSs.

practical perspectives, and waveforms which allow radars to share spectrum with communication systems without causing interference, which are very desirable for spectrum congested RF environments.

In this paper, we first showed that it is possible to realize finite alphabet constant-envelope quadrature-pulse shift keying (QPSK) MIMO radar waveforms. We proved that such the covariance matrix for QPSK waveforms is positive semi-definite and the constrained nonlinear optimization problem can be transformed into an un-constrained nonlinear optimization problem, to realize finite alphabet constant-envelope QPSK waveforms. This result is of importance for both communication and radar waveform designs where constant-envelope is highly desirable.

Second, we addressed the problem of radar waveform design for spectrally congested RF environments where radar and communication systems are sharing the same frequency band. We designed QPSK waveforms with spectrum sharing constraints. The QPSK waveform was shaped in a way that it is in the null space of communication system to avoid interference to communication system. We considered a multi-BS MIMO cellular system and

proposed algorithms for the formation of projection matrices and selection of interference channels. We designed waveforms for stationary and moving MIMO radar systems. For stationary MIMO radar we presented an algorithm for waveform design by considering the spectrum sharing constraints. Our algorithm selected the waveform capable to project maximum power at the targets. For moving MIMO radar we presented another algorithm for waveform design by considering spectrum sharing constraints. Our algorithm selected the waveform with the minimum Forbenius norm with respect to the designed waveform. This metric helped to select the projected waveform closest to the designed waveform.

APPENDIX A PRELIMINARIES

This section presents some preliminary results used in the proofs throughout the paper. For proofs of the following theorems, please see the corresponding references.

Theorem 1. *The matrix $\mathbf{A} \in \mathbb{C}^{n \times n}$ is positive semi-definite if and only if $\Re(\mathbf{A})$ is positive semi-definite [23].*

Theorem 2. *A necessary and sufficient condition for $\mathbf{A} \in \mathbb{C}^{n \times n}$ to be positive definite is that the Hermitian part*

$$\mathbf{A}_H = \frac{1}{2} [\mathbf{A} + \mathbf{A}^H]$$

be positive definite [23].

Theorem 3. *If $\mathbf{A} \in \mathbb{C}^{n \times n}$ and $\mathbf{B} \in \mathbb{C}^{n \times n}$ are positive semi-definite matrices then the matrix $\mathbf{C} = \mathbf{A} + \mathbf{B}$ is guaranteed to be positive semi-definite matrix [24].*

Theorem 4. *If the matrix $\mathbf{A} \in \mathbb{C}^{n \times n}$ is positive semi-definite then the p times Schur product of \mathbf{A} , denoted by $\mathbf{A}^{\circ p}$, will also be positive semi-definite [24].*

APPENDIX B

GENERATING CE QPSK RANDOM PROCESSES FROM GAUSSIAN RANDOM VARIABLES

Assuming identically distributed Gaussian RV's $\tilde{x}_p, \tilde{y}_p, \tilde{x}_q$ and \tilde{y}_q that are mapped onto QPSK RV's \tilde{z}_p and \tilde{z}_q using

$$\tilde{z}_p = \frac{1}{\sqrt{2}} \left[\text{sign} \left(\frac{\tilde{x}_p}{\sqrt{2}\sigma} \right) + j \text{sign} \left(\frac{\tilde{y}_p}{\sqrt{2}\sigma} \right) \right] \quad (60)$$

$$\tilde{z}_q = \frac{1}{\sqrt{2}} \left[\text{sign} \left(\frac{\tilde{x}_q}{\sqrt{2}\sigma} \right) + j \text{sign} \left(\frac{\tilde{y}_q}{\sqrt{2}\sigma} \right) \right] \quad (61)$$

where σ^2 is the variance of Gaussian RVs. The cross-correlation between QPSK and Gaussian RVs can be derived as

$$\mathbb{E}\{\tilde{z}_p \tilde{z}_q^*\} = \frac{1}{2} \mathbb{E} \left[\left\{ \text{sign} \left(\frac{\tilde{x}_p}{\sqrt{2}\sigma} \right) + j \text{sign} \left(\frac{\tilde{y}_p}{\sqrt{2}\sigma} \right) \right\} \left\{ \text{sign} \left(\frac{\tilde{x}_q}{\sqrt{2}\sigma} \right) + j \text{sign} \left(\frac{\tilde{y}_q}{\sqrt{2}\sigma} \right) \right\}^* \right]. \quad (62)$$

Using equation (13) we can write the above equation as

$$\mathbb{E}\{\tilde{z}_p \tilde{z}_q^*\} = \mathbb{E}\left\{\text{sign}\left(\frac{\tilde{x}_p}{\sqrt{2}\sigma}\right)\text{sign}\left(\frac{\tilde{x}_q}{\sqrt{2}\sigma}\right)\right\} + j \mathbb{E}\left\{\text{sign}\left(\frac{\tilde{y}_p}{\sqrt{2}\sigma}\right)\text{sign}\left(\frac{\tilde{x}_q}{\sqrt{2}\sigma}\right)\right\}. \quad (63)$$

The cross-correlation relationship between Gaussian and QPSK RVs can be derived by first considering

$$\mathbb{E}\left\{\text{sign}\left(\frac{\tilde{x}_p}{\sqrt{2}\sigma}\right)\text{sign}\left(\frac{\tilde{x}_q}{\sqrt{2}\sigma}\right)\right\} = \int_{-\infty}^{\infty} \int_{-\infty}^{\infty} \left[\text{sign}\left(\frac{\tilde{x}_p}{\sqrt{2}\sigma}\right) \times \text{sign}\left(\frac{\tilde{x}_q}{\sqrt{2}\sigma}\right) p(\tilde{x}_p, \tilde{x}_q, \rho_{\tilde{x}_p \tilde{x}_q})\right] d\tilde{x}_p d\tilde{x}_q \quad (64)$$

where $p(\tilde{x}_p, \tilde{x}_q, \rho_{\tilde{x}_p \tilde{x}_q})$ is the joint probability density function of \tilde{x}_p and \tilde{x}_q , and $\rho_{\tilde{x}_p \tilde{x}_q} = \frac{\mathbb{E}\{\tilde{x}_p \tilde{x}_q^*\}}{\sigma^2}$ is the cross-correlation coefficient of \tilde{x}_p and \tilde{x}_q . Using Hermite polynomials [25], the above double integral can be transformed as in [7]. Thus,

$$\begin{aligned} \mathbb{E}\left\{\text{sign}\left(\frac{\tilde{x}_p}{\sqrt{2}\sigma}\right)\text{sign}\left(\frac{\tilde{x}_q}{\sqrt{2}\sigma}\right)\right\} &= \sum_{n=0}^{\infty} \frac{\rho_{\tilde{x}_p \tilde{x}_q}^n}{2\pi\sigma^2 2^n n!} \times \int_{-\infty}^{\infty} \text{sign}\left(\frac{\tilde{x}_p}{\sqrt{2}\sigma}\right) e^{\tilde{x}_p^2/2\sigma^2} H_n\left(\frac{\tilde{x}_p}{\sqrt{2}\sigma}\right) d\tilde{x}_p \\ &\quad \times \int_{-\infty}^{\infty} \text{sign}\left(\frac{\tilde{x}_q}{\sqrt{2}\sigma}\right) e^{\tilde{x}_q^2/2\sigma^2} H_n\left(\frac{\tilde{x}_q}{\sqrt{2}\sigma}\right) d\tilde{x}_q \end{aligned} \quad (65)$$

where

$$H_n(\tilde{x}_m) = (-1)^n e^{\frac{\tilde{x}_m^2}{2}} \frac{d^n}{d\tilde{x}_m^n} e^{-\frac{\tilde{x}_m^2}{2}} \quad (66)$$

is the Hermite polynomial. By substituting $\hat{x}_p = \frac{\tilde{x}_p}{\sqrt{2}\sigma}$ and $\hat{x}_q = \frac{\tilde{x}_q}{\sqrt{2}\sigma}$, and splitting the limits of integration into two parts, equation (65) can be simplified as

$$\mathbb{E}\left\{\text{sign}(\hat{x}_p)\text{sign}(\hat{x}_q)\right\} = \sum_{n=0}^{\infty} \frac{\rho_{\hat{x}_p \hat{x}_q}^n}{\pi 2^n n!} \left(\int_0^{\infty} e^{\hat{x}_p^2} [H_n(\hat{x}_p) - H_n(-\hat{x}_p)] d\hat{x}_p \right)^2. \quad (67)$$

Using $H_n(-\hat{x}_p) = (-1)^n H_n(\hat{x}_p)$ [26], equation (67) can be written as

$$\mathbb{E}\left\{\text{sign}(\hat{x}_p)\text{sign}(\hat{x}_q)\right\} = \sum_{n=0}^{\infty} \frac{\rho_{\hat{x}_p \hat{x}_q}^n}{\pi 2^n n!} \left(\int_0^{\infty} e^{\hat{x}_p^2} H_n(\hat{x}_p) (1 - (-1)^n) d\hat{x}_p \right)^2. \quad (68)$$

The above equation is non-zero for odd n only, therefore, we can rewrite it as

$$\mathbb{E}\left\{\text{sign}(\hat{x}_p)\text{sign}(\hat{x}_q)\right\} = \sum_{n=0}^{\infty} \frac{\rho_{\hat{x}_p \hat{x}_q}^{2n+1}}{\pi 2^{2n} (2n+1)!} \left(\int_0^{\infty} e^{\hat{x}_p^2} H_{2n+1}(\hat{x}_p) d\hat{x}_p \right)^2. \quad (69)$$

Then using $\int_0^{\infty} e^{\hat{x}_p^2} H_{2n+1}(\hat{x}_p) d\hat{x}_p = (-1)^n \frac{(2n)!}{n!}$ from [26], we can write equation (69) as

$$\begin{aligned} \mathbb{E}\left\{\text{sign}\left(\frac{\tilde{x}_p}{\sqrt{2}\sigma}\right)\text{sign}\left(\frac{\tilde{x}_q}{\sqrt{2}\sigma}\right)\right\} &= \sum_{n=0}^{\infty} \frac{\rho_{\tilde{x}_p \tilde{x}_q}^{2n+1}}{\pi 2^{2n} (2n+1)!} \left((-1)^n \frac{2n!}{n!} \right)^2 \\ &= \frac{2}{\pi} \left[\rho_{\tilde{x}_p \tilde{x}_q} + \frac{\rho_{\tilde{x}_p \tilde{x}_q}^3}{2 \cdot 3} + \frac{1 \cdot 3 \rho_{\tilde{x}_p \tilde{x}_q}^5}{2 \cdot 4 \cdot 5} + \frac{1 \cdot 3 \cdot 5 \rho_{\tilde{x}_p \tilde{x}_q}^7}{2 \cdot 4 \cdot 6 \cdot 7} + \dots \right] \\ &= \frac{2}{\pi} \sin^{-1} \left(\mathbb{E}\{\tilde{x}_p \tilde{x}_q\} \right) \end{aligned} \quad (70)$$

In equation (64), we expanded the first part of equation (63). Now, similarly expanding the second part of equation (63), i.e.,

$$\mathbb{E}\left\{\text{sign}\left(\frac{\tilde{y}_p}{\sqrt{2}\sigma}\right)\text{sign}\left(\frac{\tilde{x}_q}{\sqrt{2}\sigma}\right)\right\} = \int_{-\infty}^{\infty} \int_{-\infty}^{\infty} \left[\text{sign}\left(\frac{\tilde{y}_p}{\sqrt{2}\sigma}\right) \text{sign}\left(\frac{\tilde{x}_q}{\sqrt{2}\sigma}\right) p(\tilde{y}_p, \tilde{x}_q, \rho_{\tilde{y}_p\tilde{x}_q})\right] d\tilde{y}_p d\tilde{x}_q \quad (71)$$

where $p(\tilde{y}_p, \tilde{x}_q, \rho_{\tilde{y}_p\tilde{x}_q})$ is the joint probability density function of \tilde{y}_p and \tilde{x}_q , and $\rho_{\tilde{y}_p\tilde{x}_q} = \frac{\mathbb{E}\{\tilde{y}_p\tilde{x}_q^*\}}{\sigma^2}$ is the cross-correlation coefficient of \tilde{y}_p and \tilde{x}_q . Using Hermite polynomials, equation (66), we can write equation (71) as

$$\begin{aligned} \mathbb{E}\left\{\text{sign}\left(\frac{\tilde{y}_p}{\sqrt{2}\sigma}\right)\text{sign}\left(\frac{\tilde{x}_q}{\sqrt{2}\sigma}\right)\right\} &= \sum_{n=0}^{\infty} \frac{\rho_{\tilde{y}_p\tilde{x}_q}^n}{2\pi\sigma^2 2^n n!} \times \int_{-\infty}^{\infty} \text{sign}\left(\frac{\tilde{y}_p}{\sqrt{2}\sigma}\right) \times e^{\tilde{y}_p^2/2\sigma^2} H_n\left(\frac{\tilde{y}_p}{\sqrt{2}\sigma}\right) d\tilde{y}_p \\ &\times \int_{-\infty}^{\infty} \text{sign}\left(\frac{\tilde{x}_q}{\sqrt{2}\sigma}\right) e^{\tilde{x}_q^2/2\sigma^2} H_n\left(\frac{\tilde{x}_q}{\sqrt{2}\sigma}\right) d\tilde{x}_q. \end{aligned} \quad (72)$$

By substituting $\hat{y}_p = \frac{\tilde{y}_p}{\sqrt{2}\sigma}$ and $\hat{x}_q = \frac{\tilde{x}_q}{\sqrt{2}\sigma}$, and splitting the limits of integration into two parts, equation (72) can be simplified as

$$\mathbb{E}\left\{\text{sign}(\hat{y}_p)\text{sign}(\hat{x}_q)\right\} = \sum_{n=0}^{\infty} \frac{\rho_{\hat{y}_p\hat{x}_q}^n}{\pi 2^n n!} \left(\int_0^{\infty} e^{\hat{y}_p^2} [H_n(\hat{y}_p) - H_n(-\hat{y}_p)] d\hat{y}_p \right)^2. \quad (73)$$

Using $H_n(-\hat{y}_p) = (-1)^n H_n(\hat{y}_p)$, above equation can be written as

$$\mathbb{E}\left\{\text{sign}(\hat{y}_p)\text{sign}(\hat{x}_q)\right\} = \sum_{n=0}^{\infty} \frac{\rho_{\hat{y}_p\hat{x}_q}^n}{\pi 2^n n!} \left(\int_0^{\infty} e^{\hat{y}_p^2} H_n(\hat{y}_p) (1 - (-1)^n) d\hat{y}_p \right)^2. \quad (74)$$

The above equation is non-zero for odd n only, therefore, we can rewrite it as

$$\mathbb{E}\left\{\text{sign}(\hat{y}_p)\text{sign}(\hat{x}_q)\right\} = \sum_{n=0}^{\infty} \frac{\rho_{\hat{y}_p\hat{x}_q}^{2n+1}}{\pi 2^{2n} (2n+1)!} \left(\int_0^{\infty} e^{\hat{y}_p^2} H_{2n+1}(\hat{y}_p) d\hat{y}_p \right)^2. \quad (75)$$

Then using $\int_0^{\infty} e^{\hat{y}_p^2} H_{2n+1}(\hat{y}_p) d\hat{y}_p = (-1)^n \frac{(2n)!}{n!}$, we can write equation (75) as

$$\begin{aligned} \mathbb{E}\left\{\text{sign}\left(\frac{\tilde{y}_p}{\sqrt{2}\sigma}\right)\text{sign}\left(\frac{\tilde{x}_q}{\sqrt{2}\sigma}\right)\right\} &= \sum_{n=0}^{\infty} \frac{\rho_{\tilde{y}_p\tilde{x}_q}^{2n+1}}{\pi 2^{2n} (2n+1)!} \left((-1)^n \frac{2n!}{n!} \right)^2 \\ &= \frac{2}{\pi} \left[\rho_{\tilde{y}_p\tilde{x}_q} + \frac{\rho_{\tilde{y}_p\tilde{x}_q}^3}{2 \cdot 3} + \frac{1 \cdot 3 \rho_{\tilde{y}_p\tilde{x}_q}^5}{2 \cdot 4 \cdot 5} + \frac{1 \cdot 3 \cdot 5 \rho_{\tilde{y}_p\tilde{x}_q}^7}{2 \cdot 4 \cdot 6 \cdot 7} + \dots \right] \\ &= \frac{2}{\pi} \sin^{-1} \left(\mathbb{E}\{\tilde{y}_p\tilde{x}_q\} \right). \end{aligned} \quad (76)$$

Combining equations (70) and (76), gives us the cross-correlation of equation (63) as

$$\mathbb{E}\{\tilde{z}_p\tilde{z}_q\} = \frac{2}{\pi} \left[\sin^{-1} \left(\mathbb{E}\{\tilde{x}_p\tilde{x}_q\} \right) + j \sin^{-1} \left(\mathbb{E}\{\tilde{y}_p\tilde{x}_q\} \right) \right]. \quad (77)$$

APPENDIX C

PROOFS

Proof of Lemma 1: To prove Lemma 1, we note that the real part of $\tilde{\mathbf{R}}_g$ is \mathbf{R}_g which is positive semi-definite by definition, thus, by Theorem 1, the complex covariance matrix $\tilde{\mathbf{R}}_g$ is also positive semi-definite. ■

Proof of Lemma 2: To prove Lemma 2, we can individually expand the sum, $\sin^{-1}(\Re(\tilde{\mathbf{R}}_g)) + j \sin^{-1}(\Im(\tilde{\mathbf{R}}_g))$, using Taylor series, i.e., first expanding $\sin^{-1}(\Re(\tilde{\mathbf{R}}_g))$

$$\sin^{-1}(\Re(\mathbf{R}_g)) = \Re(\mathbf{R}_g) + \frac{1}{2 \cdot 3} \Re(\mathbf{R}_g)_\circ^3 + \frac{1 \cdot 3}{2 \cdot 4 \cdot 5} \Re(\mathbf{R}_g)_\circ^5 + \frac{1 \cdot 3 \cdot 5}{2 \cdot 4 \cdot 6 \cdot 7} \Re(\mathbf{R}_g)_\circ^7 + \dots \quad (78)$$

Then using Theorem 3, each term or matrix, on the right hand side, is positive semi-definite, since, $\Re(\mathbf{R}_g)$ is positive semi-definite by definition. Moreover, $\sin^{-1}(\Re(\mathbf{R}_g))$ is also positive semi-definite since its a sum of positive semi-definite matrices, this follows from Theorem 1.

Similarly, expanding $j \sin^{-1}(\Im(\mathbf{R}_g))$ as

$$j \sin^{-1}(\Im(\mathbf{R}_g)) = j[\Im(\mathbf{R}_g) + \frac{1}{2 \cdot 3} \Im(\mathbf{R}_g)_\circ^3 + \frac{1 \cdot 3}{2 \cdot 4 \cdot 5} \Im(\mathbf{R}_g)_\circ^5 + \frac{1 \cdot 3 \cdot 5}{2 \cdot 4 \cdot 6 \cdot 7} \Im(\mathbf{R}_g)_\circ^7 + \dots] \quad (79)$$

Now, $\tilde{\mathbf{R}}$ is positive semi-definite since real part of it is positive semidefinite, from equation (78) and Theorem 4. ■

REFERENCES

- [1] J. Li and P. Stoica, *MIMO Radar Signal Processing*. Wiley-IEEE Press, 2008.
- [2] A. M. Haimovich, R. S. Blum, and L. J. Cimini, "MIMO Radar with Widely Separated Antennas," *IEEE Signal Processing Magazine*, vol. 25, no. 1, pp. 116–129, 2008.
- [3] J. Li and P. Stoica, "MIMO radar with colocated antennas," *IEEE Signal Processing Magazine*, vol. 24, no. 5, pp. 106–114, 2007.
- [4] J. Tan and G. Stuber, "Constant envelope multi-carrier modulation," in *MILCOM 2002. Proceedings*, vol. 1, pp. 607–611 vol.1, Oct 2002.
- [5] S. Thompson, A. Ahmed, J. Proakis, J. Zeidler, and M. Geile, "Constant envelope OFDM," *IEEE Transactions on Communications*, vol. 56, pp. 1300–1312, August 2008.
- [6] P. Stoica, J. Li, and X. Zhu, "Waveform synthesis for diversity-based transmit beampattern design," *IEEE Transactions on Signal Processing*, vol. 56, pp. 2593–2598, June 2008.
- [7] S. Ahmed, J. S. Thompson, Y. R. Petillot, and B. Mulgrew, "Finite alphabet constant-envelope waveform design for MIMO radar," *IEEE Transactions on Signal Processing*, vol. 59, no. 11, pp. 5326–5337, 2011.
- [8] S. Sodagari and A. Abdel-Hadi, "Constant envelope radar with coexisting capability with LTE communication systems," *under submission*.
- [9] The Presidents Council of Advisors on Science and Technology (PCAST), "Realizing the full potential of government-held spectrum to spur economic growth," July 2012.
- [10] Federal Communications Commission (FCC), "FCC proposes innovative small cell use in 3.5 GHz band." Online: <http://www.fcc.gov/document/fcc-proposes-innovative-small-cell-use-35-ghz-band>, December 12, 2012.
- [11] H. Shajaiah, A. Khawar, A. Abdel-Hadi, and T. C. Clancy, "Using resource allocation with carrier aggregation for spectrum sharing between radar and 4G-LTE cellular system," in *IEEE DySPAN*, 2014.
- [12] D. Fuhrmann and G. San Antonio, "Transmit beamforming for MIMO radar systems using signal cross-correlation," *IEEE Transactions on Aerospace and Electronic Systems*, vol. 44, pp. 171–186, January 2008.
- [13] T. Aittomaki and V. Koivunen, "Signal covariance matrix optimization for transmit beamforming in MIMO radars," in *in Proc. of the Forty-First Asilomar Conference on Signals, Systems and Computers (ASILOMAR)*, pp. 182–186, Nov 2007.
- [14] P. Gong, Z. Shao, G. Tu, and Q. Chen, "Transmit beampattern design based on convex optimization for {MIMO} radar systems," *Signal Processing*, vol. 94, no. 0, pp. 195 – 201, 2014.

- [15] G. Hua and S. Abeysekera, "MIMO radar transmit beam pattern design with ripple and transition band control," *IEEE Transactions on Signal Processing*, vol. 61, pp. 2963–2974, June 2013.
- [16] S. Sodagari, A. Khawar, T. C. Clancy, and R. McGwier, "A projection based approach for radar and telecommunication systems coexistence," in *IEEE Global Communications Conference (GLOBECOM)*, 2012.
- [17] A. Khawar, A. Abdel-Hadi, T. C. Clancy, and R. McGwier, "Beam pattern analysis for MIMO radar and telecommunication system coexistence," in *IEEE International Conference on Computing, Networking and Communications, Signal Processing for Communications Symposium (ICNC'14 - SPC)*, 2014.
- [18] A. Khawar, A. Abdel-Hadi, and T. C. Clancy, "MIMO radar waveform design for coexistence with cellular systems," in *2014 IEEE International Symposium on Dynamic Spectrum Access Networks: SSPARC Workshop (IEEE DySPAN 2014 - SSPARC Workshop)*, (McLean, USA), Apr. 2014.
- [19] A. Khawar, A. Abdel-Hadi, and T. C. Clancy, "Spectrum sharing between S-band radar and LTE cellular system: A spatial approach," in *2014 IEEE International Symposium on Dynamic Spectrum Access Networks: SSPARC Workshop (IEEE DySPAN 2014 - SSPARC Workshop)*, (McLean, USA), Apr. 2014.
- [20] D. Tse and P. Viswanath, *Fundamentals of Wireless Communication*. Cambridge University Press, 2005.
- [21] S. Ahmed, J. Thompson, Y. Petillot, and B. Mulgrew, "Unconstrained synthesis of covariance matrix for MIMO radar transmit beam pattern," *IEEE Transactions on Signal Processing*, vol. 59, pp. 3837–3849, aug. 2011.
- [22] A. Hyvärinen, J. Karhunen, and E. Oja, *Independent Component Analysis*. Wiley-Interscience, 2001.
- [23] D. S. Bernstein, *Matrix Mathematics: Theory, Facts, and Formulas*. Princeton University Press, second ed., 2009.
- [24] R. A. Horn and C. R. Johnson, *Matrix Analysis*. Cambridge, U.K.: Cambridge University Press, 1985.
- [25] J. Brown, Jr., "On the expansion of the bivariate gaussian probability density using results of nonlinear theory (corresp.)," *IEEE Transactions on Information Theory*, vol. 14, pp. 158–159, Sept. 1968.
- [26] A. De Maio, S. De Nicola, A. Farina, and S. Iommelli, "Adaptive detection of a signal with angle uncertainty," *IET Radar, Sonar Navigation*, vol. 4, pp. 537–547, August 2010.